

# Dynamic versus static ultra-widefield fluorescein angiography in eyes with diabetic retinopathy: a pilot prospective cross-sectional study

Hang-Qi Shen<sup>1,2,3,4,5</sup>, Jing Wang<sup>1,2,3,4,5</sup>, Tian Niu<sup>1,2,3,4,5</sup>, Ji-Li Chen<sup>6</sup>, Xun Xu<sup>1,2,3,4,5</sup>

<sup>1</sup>Department of Ophthalmology, Shanghai General Hospital, Shanghai Jiao Tong University School of Medicine, Shanghai 200080, China

<sup>2</sup>Shanghai Key Laboratory of Ocular Fundus Diseases, Shanghai General Hospital, Shanghai Jiao Tong University School of Medicine, Shanghai 200080, China

<sup>3</sup>Shanghai Engineering Center for Visual Science and Photomedicine, Shanghai General Hospital, Shanghai Jiao Tong University School of Medicine, Shanghai 200080, China

<sup>4</sup>Shanghai Engineering Center for Precise Diagnosis and Treatment of Eye Diseases, Shanghai General Hospital, Shanghai Jiao Tong University School of Medicine, Shanghai 200080, China

<sup>5</sup>National Clinical Research Center for Eye Diseases, Shanghai General Hospital, Shanghai Jiao Tong University School of Medicine, Shanghai 200080, China

<sup>6</sup>Department of Ophthalmology, Shanghai Shabei Hospital of Jing'an District, Shanghai 200435, China

**Correspondence to:** Ji-Li Chen. Department of Ophthalmology, Shanghai Shabei Hospital, No.4500 Gonghexin Road, Shanghai 200435, China. corneachen@163.com; Xun Xu. Department of Ophthalmology, Shanghai General Hospital, No.100 Haining Road, Shanghai 200080, China. drxuxun@sjtu.edu.cn

Received: 2020-11-03 Accepted: 2020-11-25

## Abstract

• **AIM:** To analyze differences in ultra-widefield fluorescein angiography (UWFA) findings between dynamic and static images of eyes with diabetic retinopathy (DR).

• **METHODS:** This cross-sectional study included 28 eyes of 28 patients with DR undergoing UWFA. A series of UWFA images acquired from each patient were converted into a time-lapse video and used as a dynamic image. A single, clear, arteriovenous phase image was chosen as a static image. Non-perfusion index (NPI) and its correlation with vascular abnormalities in different zones were compared between dynamic and static UWFA imaging.

• **RESULTS:** NPI appeared to increase from the center to the far-periphery in both groups. Dynamic NPI was lower

in the total retinal area (0.26 vs 0.29,  $P=0.009$ ) and far-periphery (0.33 vs 0.36, adjusted  $P=0.042$ ), which was contrary to the static NPI. Far-peripheral NPI was associated with intraretinal microvascular abnormality in the posterior area in both groups.

• **CONCLUSION:** Time-lapse dynamic UWFA imaging is a useful modality to differentially diagnose hypofluorescence in the most peripheral region. This modality could provide a reliable method for NPI measurement.

• **KEYWORDS:** diabetic retinopathy; ultra-widefield fluorescein angiography; non-perfusion index; time-lapse photography

**DOI:10.18240/ijo.2021.03.13**

**Citation:** Shen HQ, Wang J, Niu T, Chen JL, Xu X. Dynamic versus static ultra-widefield fluorescein angiography in eyes with diabetic retinopathy: a pilot prospective cross-sectional study. *Int J Ophthalmol* 2021;14(3):409-415

## INTRODUCTION

Diabetic retinopathy (DR) is a leading cause of visual impairment among working-age adults worldwide, occurring in approximately 35% of people with diabetes<sup>[1]</sup>. Identification of ischemic lesions, such as retinal intraretinal microvascular abnormality (IRMA), neovascularization (NV), and non-perfusion, are important in the diagnosis and the following treatment of DR. Ultra-widefield fluorescein angiography (UWFA) allows for the visualization of up to 200 degrees of the retina. This technique is more helpful than traditional fluorescein angiography techniques for the identification of peripheral ischemic lesions<sup>[2-6]</sup>. Conventionally, retinal findings are only recorded using a few typical UWFA images. Because of the spherical aberrations and different focal distances, peripheral blurring may be mistaken for non-perfusion<sup>[7]</sup>. Moreover, dynamic retinal blood circulation is represented in static pictures, which can lead to impaired identification of vascular lesions, such as subtle IRMA and NV<sup>[8]</sup>. Therefore, it is important to identify ischemic lesions more precisely.

Time-lapse photography is a cinematography technique which creates dynamic videos from a series of still images. So far, it

has been demonstrated to be useful for monitoring neuronal development<sup>[9]</sup> and clinical practice<sup>[10-11]</sup>. In ophthalmology, Querques *et al*<sup>[12]</sup> re-created an automatic pseudo-movie from five static fluorescein angiography pictures, sharing the visualization of dye leakage in macular degeneration. Gentile *et al*<sup>[13]</sup> reported cases of idiopathic macular holes and illustrated the pathogenesis, progression, and surgical closure by morphing serial optical coherence tomography scans into a movie format. We have previously described dynamic angiography through a few typical videos<sup>[14]</sup>. But no studies have implemented dynamic UWFA to explore the distribution of ischemic lesions in DR eyes.

In this study, we hypothesized that a time-lapse dynamic UWFA video presenting the complete angiography process might be of significant value in DR diagnosis. We compared the distribution of non-perfusion index (NPI) in different retinal zones between dynamic videos and static images and investigated its correlation with vascular abnormalities in eyes with DR.

## SUBJECTS AND METHODS

**Ethical Approval** This pilot prospective, cross-sectional study was conducted at Shanghai General Hospital between January 2017 and December 2019. It conformed to the tenets of the Declaration of Helsinki, and the data collection and analysis were approved by the Medical Ethics Committee of Shanghai General Hospital, Shanghai Jiao Tong University School of Medicine. Written informed consent for participation in the study was obtained from each patient before imaging.

**Subjects** The inclusion criteria for patients recruited in the study were as follows: 1) age: 18y or older with a primary diagnosis of diabetes mellitus; and 2) presence of DR. The exclusion criteria were as follows: 1) ocular comorbidities (such as retinal vein and artery occlusion, ocular tumors or uveitis); 2) lack of clear images because of significant media opacities (such as cataract, vitreous hemorrhage); 3) poor patient cooperation; and 4) allergy to fluorescein.

**Image Capture and Processing** All eyes were dilated with Mydrin-P (0.5% phenylephrine hydrochloride and 0.5% tropicamide; Santen Pharmaceuticals, Japan) three doses at an interval of 5min for a better acquisition of high-quality images<sup>[7,15]</sup>. UWFA was performed 30min after the last eye drop administration. Each patient received an intravenous injection of 5-mL of 10% sodium fluorescein. After intravenous administration of fluorescein dye, UWFA (Optos PLC, Dunfermline, United Kingdom) images were acquired by a trained ophthalmology technician. Each patient had one random eye used for the time-lapse imaging of retinal angiogenesis. The time-lapse imaging protocols were as follows: images were recorded every 2s in the early phases (within 60s), every 10s in the mid phases (61-300s), and every 15s in the late phases (301-600s). UWFA in the other eye was

performed as per the protocol for conventional angiography. The technician was allowed to adjust the recording times without compromising the conventional angiography in the contralateral eyes.

Images were exported as high-quality Joint Photographic Experts Group format and imported into Adobe software (Adobe Photoshop CC, Adobe Photoshop Lightroom and Adobe After Effects, Adobe Systems Inc, San Jose, California, USA). Poor-quality images because of eye movements or blinking were removed. The retina was divided into three concentric zones (posterior region, mid-periphery, and far-periphery) and four quadrants (superior, inferior, temporal, and nasal quadrants; Figure 1). The ratio of the horizontal and vertical axes of the concentric ellipses was set at 1.2:1 based on the quantification of the Optos 200Tx images evaluated by Oishi *et al*<sup>[16]</sup>.

**Measurements** Two independent, trained examiners assessed the presence of the following lesions: non-perfusion area (NPA, area of a darker appearance of background fluorescence flanked by adjacent arterioles and/or capillaries caused by the absence of retinal arterioles and/or capillaries), IRMA (defined as tortuous intraretinal vascular segment), and NV (area of early hyperfluorescence caused by leakage). Disagreements were reviewed by open adjudication with a senior examiner. A single clear arteriovenous phase (between 45s and 90s) image was chosen for annotation and analysis as the static UWFA image, and was analyzed for the number of IRMAs, NVs, and NPA. The NPA was manually outlined and calculated based on the number of pixels. Since the outline of the NPA on UWFA could be challenging to decipher, images were zoomed in and the brightness was adjusted to optimize the images in Adobe software. The results of two independent examiners were averaged to obtain final values for subsequent analysis.

Serial angiographic frames from the same examination were required to generate the time-lapse dynamic UWFA video as a Moving Picture Experts Group 4 file, as the dynamic UWFA image. The examiners obtained the dynamic videos and marked areas of hypofluorescence flanked by adjacent arterioles and/or capillaries, designating them as dynamic NPA (Video 1, online supplementary). To reduce errors (as the NPA size in pixels could be varied in a series of angiographic frames due to subtle differences in shooting positions), non-perfusion zones on the dynamic and static images of one testing eye were marked on the same original arteriovenous phase image (Figure 2). The dynamic NPI was defined as the ratio of the dynamic NPA to the UWFA retinal area. The static NPI was defined as the ratio of the static NPA to the UWFA retinal area. The global NPI (the ratio of the global NPA to the entire UWFA visible retinal area) and NPI within each of three concentric zones and four quadrants (the ratio of the regional

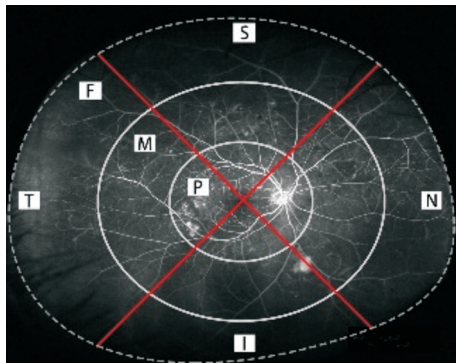


**Figure 1 UWFA imaging of a right eye** The retina was divided into compartments. The posterior pole zone (P) and mid-peripheral zone (M) were demarcated by a concentric grey ellipse (1.2:1) centered on the fovea, and the far-peripheral zone's (F) boundaries were demarcated by the outer grey ellipse and the edge of the image (shown as the grey dotted borders). Four quadrants, namely the superior (S), inferior (I), temporal (T), and nasal (N) quadrants, were demarcated with red lines.

NPA to the area of the region) were calculated and compared between the dynamic and static modalities<sup>[17-18]</sup>.

**Statistical Analysis** Statistical analyses were performed using SPSS Statistics (version 23.0; IBM Corp, Armonk, New York, USA). The intraclass correlation coefficients (ICC) were used to assess the agreement between examiners, and ICC values greater than 0.80 were considered reflective of good agreement. The normality of the distribution of the continuous variable was assessed using a Shapiro-Wilk test. Multiple groups (>2) were compared using a one-way analysis of variance (ANOVA) or Friedman test (when the ANOVA test was not applicable). Multiple comparisons were done using the false discovery rate. The Wilcoxon signed-rank test was used to compare the correlation between static NPI and dynamic NPI. Bland-Altman plots were used to assess the comparability of two measures. A *P* value below 0.05 was considered statistically significant.

## RESULTS

**Demographic Features of the Study Eyes** Twenty-eight patients with a primary diagnosis of DR were included in the study (Table 1). Four eyes had received panretinal photocoagulation. An average of 62.2±5.1 images were captured in each eye. After removal of poor-quality images, an average of 60.5±5.2 images were included for the analyses.

**Non-Perfusion Index on Dynamic and Static UWFA** Across three concentric regions, NPI was found to be highest in the far-peripheral regions and lowest in the posterior regions in both dynamic and static groups (*P*=0.001 and *P*=0.007 respectively). Across the four quadrants in these eyes, there was a statistically significant difference in static NPI (*P*=0.008), but not in dynamic NPI (*P*=0.081).

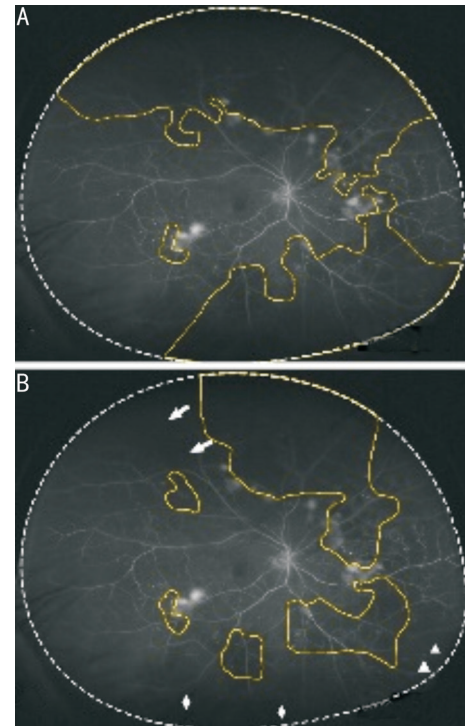


**Figure 2 Delineation of the NPA in static and dynamic UWFA imaging** The NPA was outlined in yellow as regional hypofluorescence relative to the background, flanked by neighboring filled vessels. A: The NPA was outlined based on a single image; B: The NPA was outlined based on a time-lapse dynamic video. Hypofluorescence in the peripheral region of the retina caused by low image contrast (triangles), the eyelash artifact (rhombus), and cataract (arrows) were related to a larger non-perfusion region. Videos are helpful for the differential diagnosis of hypofluorescence.

Table 1 Patient characteristics	mean±SD (range)
Basic demographics (n=28)	Values
Female gender, n (%)	13 (46.4)
Mean age (y)	63.8±10.1 (39-82)
Mean diabetes duration (y)	15.0±5.7 (1-30)
Diabetes type (type 1/type 2)	0/28
Study eye (right/left)	11/17
Total eyes, n (%)	
Mild NPDR	5 (17.9)
Moderate NPDR	5 (17.9)
Severe NPDR	7 (25.0)
PDR	11 (39.2)
DR features, n (%)	
IRMA	17 (60.7)
NV	7 (25.0)
NPA	17 (60.7)

NPDR: Nonproliferative diabetic retinopathy; PDR: Proliferative diabetic retinopathy; DR: Diabetic retinopathy; IRMA: Intraretinal microvascular abnormalities; NV: Neovascularization; NPA: Non-perfusion area.

**Table 2 Correlation between dynamic and static NPI on UWFA**

Parameters	Dynamic NPI	Static NPI	<i>P</i>	Adjusted <i>P</i>
Total	0.26±0.29 (0.15, 0.04-0.42)	0.29±0.30 (0.18, 0.06-0.53)	0.009	
Concentric regions				
Posterior	0.06±0.08 (0.03, 0.06-0.09)	0.10±0.14 (0.04, 0.01-0.20)	0.016	0.056
Mid-periphery	0.24±0.31 (0.10, 0.05-0.35)	0.26±0.31 (0.11, 0.05-0.41)	0.047	0.082
Far-periphery	0.33±0.33 (0.23, 0.04-0.56)	0.36±0.35 (0.25, 0.06-0.69)	0.006	0.042
Quadrants				
Superior	0.27±0.33 (0.11, 0-0.56)	0.34±0.38 (0.21, 0.01-0.73)	0.046	0.107
Inferior	0.30±0.34 (0.09, 0.02-0.66)	0.33±0.35 (0.18, 0.03-0.58)	0.570	0.570
Nasal	0.31±0.28 (0.22, 0.07-0.58)	0.33±0.29 (0.23, 0.09-0.69)	0.233	0.272
Temporal	0.18±0.31 (0.03, 0-0.14)	0.19±0.30 (0.09, 0-0.22)	0.071	0.099

Numeric data are presented as mean±SD (median, interquartile range). *P* values were calculated using the Wilcoxon signed-rank test and the False Discovery Rate was used to correct for multiple testing. NPI: Non-perfusion index.

**Table 3 Factors influencing the identification of non-perfusion in static UWFA images**

Patient No.	DR grade	Unclear ocular media	Eye movement	Subretinal hemorrhage	Unrecognizable hypofluorescence in periphery
4	Moderate NPDR	-	-	-	-
2	Severe NPDR	-	+	-	-
13	Severe NPDR	-	-	-	-
14	Severe NPDR	-	-	-	+
20	Severe NPDR	-	-	-	+
24	Severe NPDR	+	-	-	+
25	Severe NPDR	-	-	-	+
28	Severe NPDR	-	-	-	-
3	PDR	-	+	+	-
6	PDR	-	-	-	+
8	PDR	+	-	-	+
9	PDR	-	-	-	-
11	PDR	-	-	-	+
12	PDR	-	-	-	-
16	PDR	+	-	-	-
17	PDR	-	-	-	+
22	PDR	-	-	-	-
<i>n</i> (%)		3 (17.6)	2 (11.8)	1 (5.9)	8 (47.1)

DR: Diabetic retinopathy; NPDR: Nonproliferative diabetic retinopathy; PDR: Proliferative diabetic retinopathy; +: Exist; -: Not exist.

Regional distributions of dynamic and static NPI from the same eye are compared in Table 2. Dynamic NPI appeared to be lower in the total retinal area (*P*=0.009) and far-periphery (adjusted *P*=0.042) in contrast to static NPI. Factors influencing the identification of NPI in static images are listed in Table 3. The leading factor was unrecognizable hypofluorescence in periphery (47.1%), followed by unclear ocular media (17.6%). The mean difference between dynamic and static NPI was 2.74%±4.81% (range -12.17% to 6.70%; Figure 3).

**Correlation of Non-Perfusion Index and Vascular Abnormalities** IRMAs and NVs were most prevalent in the mid-periphery (*P*=0.004 and *P*=0.03, respectively). The posterior segment IRMA quantity was correlated with both

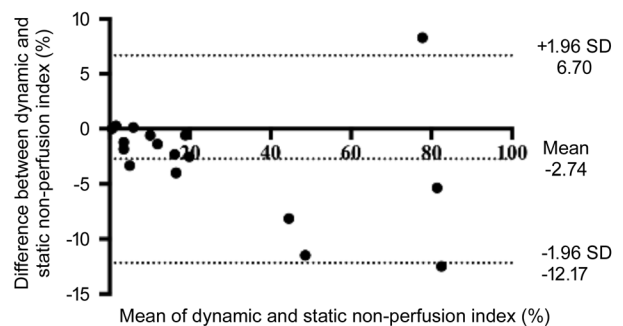


**Figure 3 Bland-Altman plot of the dynamic and static NPI** This plot presents the agreement between dynamic and static NPI in the total retinal area. The mean difference between dynamic and static NPI was 2.74%±4.81%. The limits of agreement are -12.17% and 6.70%.

dynamic and static far-peripheral NPI ( $R=0.526$ ,  $P=0.036$ ; and  $R=0.517$ ,  $P=0.040$ , respectively; Table 4). There was no correlation between far-periphery NPI and NV in both groups ( $P>0.05$ , range 0.137-0.360).

The ICCs between examiners were 0.936 for IRMA, 0.964 for NV and 0.977 for NPI.

## DISCUSSION

With advances in imaging technology, the development of fundus angiography from static to dynamic is an inevitable trend. In previous studies, it has been proven to be useful in visualizing abnormal vasculature leakage<sup>[12]</sup> and illustrating the progression of macular hole<sup>[13]</sup>. The present study used a time-lapse technique to visualize the complete UWFA process in patients with DR. Compared to static NPI, dynamic NPI generated using a time-lapse technique was significantly lower in the total retina (0.26 vs 0.29,  $P=0.009$ ) and far-periphery (0.33 vs 0.36, adjusted  $P=0.042$ ). The far-periphery NPI was associated with posterior segment IRMA quantity in both groups.

NPI appeared to increase from the center to the periphery in both groups. The lower perfusion pressure at further distances from the posterior pole may cause a higher NPI in the peripheral retina<sup>[19]</sup>. We noticed that NPI could be quite variable. The NPI in Son *et al*'s<sup>[20]</sup> study was found to be highest in the temporal quadrant and lowest in the superior quadrant, with a global NPI of 0.59. In Silva *et al*'s<sup>[18]</sup> study, the NPI was observed to be the highest in the modified superotemporal quadrant. On one hand, variable NPI values may be caused by the different grading protocols and study characteristics. On the other hand, areas of hypofluorescence is a nonspecific hallmark on static images, which can be related to non-perfusion, subretinal hemorrhage or vitreous opacity.

The present study showed significant differences between dynamic and static NPI in the far-periphery. Our results demonstrated that low image contrast and eyelash artifact in the most peripheral region in UWFA imaging can contribute to a higher NPI. Some non-perfusion in peripheral retinal zones may actually be perfused. We considered that a 2.74% NPI may be an overestimation when calculated on a single UWFA image. In comparison with static pictures, videos are helpful for the differential diagnosis of hypofluorescence and for providing more information with regard to the peripheral retina.

We observed that the highest NPI was in the far-periphery, while IRMAs and NV occurred more frequently in the mid-periphery and posterior area. Analysis by Spearman's rank correlation showed the severity of non-perfusion in the peripheral zone was associated with the prevalence of IRMAs in the posterior zone. These results indicate that the ischemia-induced vascular abnormalities usually occurs at the border

**Table 4 Correlations between far-peripheral NPI and IRMA and between far-peripheral NPI and NV in dynamic and static UWFA**

Parameters	IRMA		NV	
	R	P	R	P
Dynamic				
Total	0.306	0.250	0.680	0.137
Posterior	0.526 <sup>a</sup>	0.036 <sup>a</sup>	0.534	0.275
Mid-periphery	0.240	0.370	0.640	0.171
Far-periphery	-0.047	0.862	0.530	0.279
Static				
Total	0.229	0.394	0.539	0.270
Posterior	0.517 <sup>a</sup>	0.040 <sup>a</sup>	0.519	0.291
Mid-periphery	0.147	0.586	0.459	0.360
Far-periphery	-0.217	0.419	0.496	0.317

R: Spearman correlation coefficient. P values were calculated using a linear Spearman's correlation. <sup>a</sup> $P<0.05$ , statistically significance. NPI: Non-perfusion index; IRMA: Intraretinal microvascular abnormality; NV: Neovascularisation.

between the perfusion and NPA, in concordance with previous study<sup>[21]</sup>. Lange *et al*<sup>[22]</sup> found that far-peripheral NPI was significantly associated with mid-peripheral NV index (linear regression:  $Y=0.103X+0.841$ ,  $P=0.007$ ). Son *et al*<sup>[20]</sup> found that the total NV quantity was associated with posterior segment NPI ( $R=0.416$ ,  $P=0.009$ ), but was not associated with NPI in the entire UWFA area or other regional areas ( $P>0.05$ , range 0.299-0.982).

The present study demonstrated that dynamic UWFA imaging allows for the reliable measurement of retinal non-perfusion. As a result, the precise application of panretinal photocoagulation and targeted retinal photocoagulation based on accurate non-perfusion delineation may be possible. An additional advantage is that a time-lapse video formed by a sequence of UWFA images is more likely helpful in differentiating retinal vascular lesions (Video 2, online supplementary). While leakage on fluorescein angiography conventionally helps to evaluate NV activity<sup>[8]</sup>, a single image may be insufficient to distinguish NV from other lesions causing leakage, such as IRMA or other vascular abnormalities (Figure 4). Therefore, with regard to clinical and scholarly presentations, active classic NV of the disc and NV elsewhere could be easily detected in the videos (arrows in Video 3, online supplementary). Vascular leakage, non-perfusion, and granular background fluorescence at the far periphery, with increasing hyperfluorescence in the late phase, were clearly detected (arrows in Video 4, online supplementary). In addition, the UWFA time-lapse imaging allowed the posterior vitreous detachment with a Weiss ring as hypofluorescence at the posterior pole (arrows in Video 5, online supplementary). The strength of this study lies in the fact that we assessed the value of dynamic UWFA imaging in reliable identification of

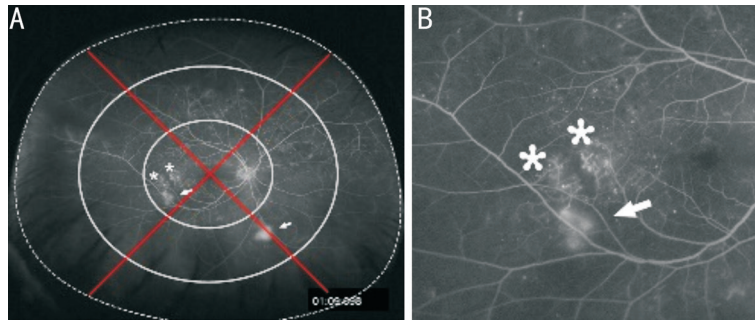


**Figure 4 Intraretinal microvascular abnormalities and NV in UWFA** A: Intraretinal microvascular abnormalities (starred polygons) and NV (arrows) were outlined on the total visible retina; B: A region of the imaging. A single image may be insufficient to distinguish NV from intraretinal microvascular abnormalities as both of lesions can cause leakage.

peripheral retinal non-perfusion and vascular abnormalities in DR. A time-lapse video has the ability to integrate information, thereby synthesizing these isolated and less informative images, reflecting the real dynamic display process in fundus vessels. In addition, the images were analyzed, and the retinas were graded by two independent examiners.

Limitations of this study include the small number of patients. Besides, our study did not correct the peripheral warp present in UWFA. Since the most peripheral part of a UWFA image is magnified, we evaluated retinal non-perfusion using NPI instead of evaluating absolute areas of non-perfusion. Tan *et al*<sup>[23]</sup> used stereographic projection software to calculate precise NPA (in mm<sup>2</sup>) and compared corrected NPI to original NPI. They found that corrected NPI correlated with original NPI (Spearman correlation  $R=0.978$ ,  $P<0.001$ ), with no significant difference between the two NPI values (Wilcoxon signed-rank test,  $P=0.239$ ). Therefore, we believe that the discrepancy in NPI values may not significantly alter our conclusions. In addition, this technique requires patients to maintain good fixation long enough to attain high-quality images, which can be modified with the development of imaging technology.

In summary, we conclude that a dynamic UWFA video helps to improve the diagnostic accuracy of DR. Further studies are warranted to reveal the potential value of treatment and follow-up of DR patients. It should be noted that whether UWFA will attain a key position as a clinically relevant and irreplaceable tool remains unknown. Future studies, including the ongoing Intravitreal Aflibercept as Indicated by Real-Time Objective Imaging to Achieve Diabetic Retinopathy Improvement (registered at <http://www.clinicaltrials.gov>, with a registration number of NCT03531294) and Peripheral Diabetic Retinopathy Lesions on Ultrawide-field Fundus Images and Risk of DR Worsening over Time (DRCR.net, Protocol AA)<sup>[24]</sup>, will help shed light on the potential role of UWFA findings in the evaluation and clinical management of DR eyes.

#### ACKNOWLEDGEMENTS

The authors thank Dr. Junyan Zhang (Bothwin Clinical Study Consultant, Redmond, WA, USA) and Dr. Wenrui Ma

(Shanghai Fudan University, Shanghai, China) for their helpful review and advice for this manuscript.

**Authors' contributions:** Shen HQ performed the experiments, and was a major contributor in writing the manuscript. Wang J and Niu T analyzed and interpreted the patient data. Chen JL and Xu X edited and revised manuscript. All authors read and approved the final manuscript.

**Foundations:** Supported by National Natural Science Foundation of China (No.81570851); Project of Shanghai Medical Key Specialty Construction (No.ZK2019B27); National Project of Shanghai Municipal Commission of Health and Family Planning (No.201740001); Project of Shanghai Jingan District Municipal Commission of Health and Family Planning (No.2018MS12); Advanced and Appropriate Technology Promotion Project of Shanghai Health Commission (No.2019SY012); Shanghai Jiao Tong University Translation Medicine Cross Research Fund Project (No. YG2019QNA61).

**Conflicts of Interest:** Shen HQ, None; Wang J, None; Niu T, None; Chen JL, None; Xu X, None.

#### REFERENCES

- 1 Ting DS, Cheung GC, Wong TY. Diabetic retinopathy: global prevalence, major risk factors, screening practices and public health challenges: a review. *Clin Exp Ophthalmol* 2016;44(4):260-277.
- 2 Friberg TR, Pandya A, Eller AW. Non-mydratric panoramic fundus imaging using a non-contact scanning laser-based system. *Ophthalmic Surg Lasers Imaging* 2003;34(6):488-497.
- 3 Wessel MM, Aaker GD, Parlitsis G, Cho M, D'Amico DJ, Kiss S. Ultra-wide-field angiography improves the detection and classification of diabetic retinopathy. *Retina* 2012;32(4):785-791.
- 4 Price LD, Au S, Chong NV. Optomap ultrawide field imaging identifies additional retinal abnormalities in patients with diabetic retinopathy. *Clin Ophthalmol* 2015;9:527-531.
- 5 Silva PS, Cavallerano JD, Haddad NM, Kwak H, Dyer KH, Omar AF, Shikari H, Aiello LM, Sun JK, Aiello LP. Peripheral lesions identified on ultrawide field imaging predict increased risk of diabetic retinopathy progression over 4 years. *Ophthalmology* 2015;122(5):949-956.

- 6 Sears CM, Nittala MG, Jayadev C, Verhoeck M, Fleming A, van Hemert J, Tsui I, Sadda SR. Comparison of subjective assessment and precise quantitative assessment of lesion distribution in diabetic retinopathy. *JAMA Ophthalmol* 2018;136(4):365-371.
- 7 Silva PS, Cavallerano JD, Sun JK, Soliman AZ, Aiello LM, Aiello LP. Peripheral lesions identified by mydriatic ultrawide field imaging: distribution and potential impact on diabetic retinopathy severity. *Ophthalmology* 2013;120(12):2587-2595.
- 8 Lee CS, Lee AY, Sim DA, Keane PA, Mehta H, Zarranz-Ventura J, Fruttiger M, Egan CA, Tufail A. Reevaluating the definition of intraretinal microvascular abnormalities and neovascularization elsewhere in diabetic retinopathy using optical coherence tomography and fluorescein angiography. *Am J Ophthalmol* 2015;159(1):101-110.e1.
- 9 Kay JN, Roeser T, Mumm JS, Godinho L, Mrejeru A, Wong RO, Baier H. Transient requirement for ganglion cells during assembly of retinal synaptic layers. *Development* 2004;131(6):1331-1342.
- 10 Insua MF, Cobo AC, Larreategui Z, Ferrando M, Serra V, Meseguer M. Obstetric and perinatal outcomes of pregnancies conceived with embryos cultured in a time-lapse monitoring system. *Fertil Steril* 2017;108(3):498-504.
- 11 Kirkegaard K, Hindkjaer JJ, Grøndahl ML, Kesmodel US, Ingerslev HJ. A randomized clinical trial comparing embryo culture in a conventional incubator with a time-lapse incubator. *J Assist Reprod Genet* 2012;29(6):565-572.
- 12 Querques G, Soubrane G, Souied EH, Delle Noci N. A new approach for visualisation of dye leakage in fluorescein angiography. *Br J Ophthalmol* 2007;91(12):1685.
- 13 Gentile RC, Landa G, Pons ME, Elliott D, Rosen RB. Macular hole formation, progression, and surgical repair: case series of serial optical coherence tomography and time lapse morphing video study. *BMC Ophthalmol* 2010;10:24.
- 14 Gu CF, Chen JL, Su T, Qiu QH. Time-lapse angiography of the ocular fundus: a new video-angiography. *BMC Med Imaging* 2019;19(1):98.
- 15 Lu J, Mai GY, Luo Y, Li M, Cao D, Wang X, Yan H, Sadda SR, Lu L. Appearance of far peripheral retina in normal eyes by ultra-widefield fluorescein angiography. *Am J Ophthalmol* 2017;173:84-90.
- 16 Oishi A, Hidaka J, Yoshimura N. Quantification of the image obtained with a wide-field scanning ophthalmoscope. *Investig Ophthalmol Vis Sci* 2014;55(4):2424-2431.
- 17 Tsui I, Kaines A, Havunjian MA, Hubschman S, Heilweil G, Prasad PS, Oliver SC, Yu F, Bitrian E, Hubschman JP, Friberg T, Schwartz SD. Ischemic index and neovascularization in central retinal vein occlusion. *Retina* 2011;31(1):105-110.
- 18 Silva PS, Dela Cruz AJ, Ledesma MG, van Hemert J, Radwan A, Cavallerano JD, Aiello LM, Sun JK, Aiello LP. Diabetic retinopathy severity and peripheral lesions are associated with nonperfusion on ultrawide field angiography. *Ophthalmology* 2015;122(12):2465-2472.
- 19 Fan W, Nittala MG, Velaga SB, Hirano T, Wykoff CC, Ip M, Lampen SIR, van Hemert J, Fleming A, Verhoeck M, Sadda SR. Distribution of nonperfusion and neovascularization on ultrawide-field fluorescein angiography in proliferative diabetic retinopathy (RECOVERY study): report 1. *Am J Ophthalmol* 2019;206:154-160.
- 20 Son G, Kim YJ, Sung YS, Park B, Kim JG. Analysis of quantitative correlations between microaneurysm, ischaemic index and new vessels in ultrawide-field fluorescein angiography images using automated software. *Br J Ophthalmol* 2019;103(12):1759-1764.
- 21 Early Treatment Diabetic Retinopathy Study Research Group. Fundus photographic risk factors for progression of diabetic retinopathy. ETDRS report number 12. *Ophthalmology* 1991;98(5):823-833.
- 22 Lange J, Hadziahmetovic M, Zhang JF, Li WY. Region-specific ischemia, neovascularization and macular oedema in treatment-naïve proliferative diabetic retinopathy. *Clin Exp Ophthalmol* 2018;46(7):757-766.
- 23 Tan CS, Chew MC, van Hemert J, Singer MA, Bell D, Sadda SR. Measuring the precise area of peripheral retinal non-perfusion using ultra-widefield imaging and its correlation with the ischaemic index. *Br J Ophthalmol* 2016;100(2):235-239.
- 24 Gella L, Raman R, Kulothungan V, Sharma T. Prevalence of posterior vitreous detachment in the population with type II diabetes mellitus and its effect on diabetic retinopathy: Sankara Nethralaya Diabetic Retinopathy Epidemiology and Molecular Genetic Study SN-DREAMS report no. 23. *Jpn J Ophthalmol* 2012;56(3):262-267.